# Effect of the Dianhydride/Branched Diamine Ratio on the Architecture and Room Temperature Healing Behavior of Polyetherimides

Susa, Arijana; Bose, Ranjita; Grande, Antonio; van der Zwaag, Sybrand; Garcia Espallargas, Santiago

**DOI**
10.1021/acsami.6b10433

**Publication date**
2016

**Document Version**
Accepted author manuscript

**Published in**
ACS Applied Materials and Interfaces

**Citation (APA)**
Susa, A., Bose, R., Grande, A., van der Zwaag, S., & Garcia Espallargas, S. (2016). Effect of the Dianhydride/Branched Diamine Ratio on the Architecture and Room Temperature Healing Behavior of Polyetherimides. *ACS Applied Materials and Interfaces*, *8*(49), 34068−34079. Article 10433. https://doi.org/10.1021/acsami.6b10433

Doi: 10.1021/acsami.6b10433
ACS Appl. Mater. Interfaces, 2016, 8 (49), pp 34068–34079

# Effect of the dianhydride/branched diamine ratio on the architecture and room temperature healing behavior of polyetherimides

A. Susa, R. K. Bose, A. M. Grande, S. van der Zwaag, S. J. Garcia*

Novel Aerospace Materials group, Faculty of Aerospace Engineering,

Delft University of Technology, Kluyverweg 1, 2629 HS, Delft, The Netherlands

*e-mail: s.j.garciaespallargas@tudelft.nl*

**Abstract**

Traditional polyetherimides (PEIs) are commonly synthesized from an aromatic diamine and an aromatic dianhydride (e.g. 3,4'-oxydianiline (ODA) and 4,4'-oxydiphtalic anhydride (ODPA)) leading to the imide linkage and outstanding chemical, thermal and mechanical properties yet lacking any self-healing functionality. In this work, we have replaced the traditional aromatic diamine by a branched aliphatic fatty dimer diamine (DD1). This led to a whole family of self-healing polymers not containing reversible chemical bonds, capable of healing at (near) room temperature yet maintaining very high elastomeric-like mechanical properties (up to 6 MPa stress and 570% strain at break). In this work, we present the effect of the DD1/ODPA ratio on the general performance and healing behavior of a room temperature healing polyetherimide. A dedicated analysis suggests that healing proceeds in three steps: (i) an initial adhesive step leading to the formation of a relatively weak interface; (ii) a second step at long healing times leading to the formation of an interphase with different properties than the bulk material and (iii) disappearance of the damaged zone leading to full healing. We argue that the fast interfacial adhesive step is due to van der Waals interactions of long dangling alkyl chains followed by an interphase formation due to polymer chain interdiffusion. An increase in DD1 ratio leads to an increase in the healing kinetics and displacement shift of the first healing step towards lower temperatures. An excess of DD1 leads to the crosslinking of the polymer thereby restricting the necessary mobility for the interphase formation and limiting the self-healing behavior. The results here presented offer a new route for the development of room temperature self-healing thermoplastic elastomers with improved mechanical properties using fatty dimer diamines.

Keywords: *polyetherimide, self-healing, fatty dimer diamine, interface healing, branched polymer, interdiffusion, dangling chains*

## 1. Introduction

The field of intrinsic self-healing polymers increasingly focuses on the use of different types of reversible covalent and non-covalent bonds, such as disulfide linkages, hydrogen bonds and ionic interactions (1-3). Since reversible bonds are weaker than their non-reversible counterparts, self-healing polymers generally show relatively low mechanical properties when they heal at room temperature or need energy input (heating) in case of variants with a higher strength. Room temperature self-healing polymers with high mechanical properties are yet to be developed (1, 4, 5). To do so the role of the polymer architecture is crucial for balancing healing and mechanical properties (6). In this respect, starting from a high performance polymer to implement the self-healing characteristics is the strategy we use here.

In the present work we use polyimides as the starting material to develop polymers capable of autonomous self-healing at room temperature yet having good mechanical properties. Aromatic polyimides (PIs) have been widely used in highly demanding applications for decades due to their thermal stability, chemical resistance, high glass-transition temperature and mechanical integrity. Rigid aromatic backbones are known to be responsible for the high thermal stability and mechanical properties of PIs. Properties of PIs can be tailored by macromolecular architecture modification using various rigid and flexible monomers (cycloaliphatic, aliphatic) as the molecular dynamics are altogether decided by the combination of molecular packing (e.g. charge transfer complexes, CTC) and chain motions (7, 8) with aliphatic groups generally disrupting the molecular packing (9). As in many other material classes, the traditional approach to increase the service life of polyimides has been by increasing their thermal and mechanical stability (10-12). However, a small amount of work has already been done on turning polyimides into self-healing grades. Nevertheless, these efforts have not been very successful so far and resulted in polymers with low mechanical properties or needing heating to induce healing (13-16).

In a recent work (17, 18), we proposed the use of a long chain aliphatic branched fatty dimer diamine (DD1) to develop intrinsic room temperature healing polyimides by polycondensation. The approach consisted in the partial or full replacement of the traditional aromatic diamine (3,4'-oxydianiline (3,4'-ODA)) by DD1 maintaining the dianhydride used in traditional synthesis of LaRC$^{TM}$-IA type polyetherimide (4,4'-oxydiphthalic anhydride (ODPA)). Interestingly, other groups have also recently reported fatty dimer building blocks in the creation of

self-healing polymers although in these cases the healing capabilities were implemented by non-covalent interactions such as H-bonds and ionic interactions. For instance, Cordier et al. used fatty diacids and triacids to obtain a self-healing thermoreversible rubber from supramolecular assembly, with the hydrogen bonding as healing mechanism (19). Lutz et al. developed a shape-recovery PU–acrylate-based coating with thermally activated self-healing ability using a fatty dimer diol with recrystallization as the mechanism responsible for healing (20). While Aboudzadeh et al. synthesized fully bio based supramolecular networks with room temperature self-healing ability based on reversible ionic interactions between DD1 and different carboxylic acids (21). A different approach based on physical healing was followed by Yamaguchi et al. (22-24). In their work, healing was attributed to entanglement couplings and interdiffusion of un-reacted chain-ends in non-branched soft polymer gels.

In this paper we show for the first time that the dangling chains in branched polymers (i.e. branches) can be responsible for full physical healing of strong polymers, without requiring other non-covalent interactions. Starting from DD1 branched diamine and a standard aromatic dianhydride, we have developed room temperature intrinsic self-healing polyetherimides with high mechanical properties. In this work, we investigate the effect of the aliphatic diamine to aromatic dianhydride ratio on the general polymer properties and healing behavior by means of mechanical and rheological testing. Such an approach enabled the identification and quantification of different molecular processes influencing macroscopic healing (cut-heal). The results show a high dependence of healing on the hydrophobic alkyl groups of the long branches of the aliphatic diamine.

## 2. Experimental

### 2.1. Synthesis

Four different polyimides were synthesized using a two-step polymerization process as described below. The monomers used (Scheme 1) were an aromatic dianhydride 4,4'-oxydiphthalic anhydride (ODPA) (98%, TCI Europe N.V.) and a fatty dimer diamine derived from vegetable oil (DD1) (Croda Nederland B.V.). Both monomers were used as received ($^1$H NMR spectra of the monomers is shown in Figure S2, SI). DD1 is a mixture of mostly saturated C36 isomers with close to 100% amine difunctionality. Four polymers with different DD1/ODPA molar ratios with respect to the theoretical stoichiometric ratio were synthesized: **D-0.9** (with 10 mol.% excess of ODPA), **D-1.0** (at the theoretical stoichiometric ratio DD1/ODPA), **D-1.1** (with 10 mol.% excess of DD1) and **D-1.2** (with 20 mol.% excess of DD1). The amounts of each monomer were calculated according to the molecular weights of the monomers ($MW_{ODPA}$=310.20 g/mol and $MW_{DD1}$=536.80 g/mol) and assuming both chemicals are 100% difunctional. The synthesis was conducted in N,N-dimethylacetamide (DMAc, 99.5% extra dry, Acros Organics) polar aprotic solvent with total solids (monomers) content of 20 wt.%.

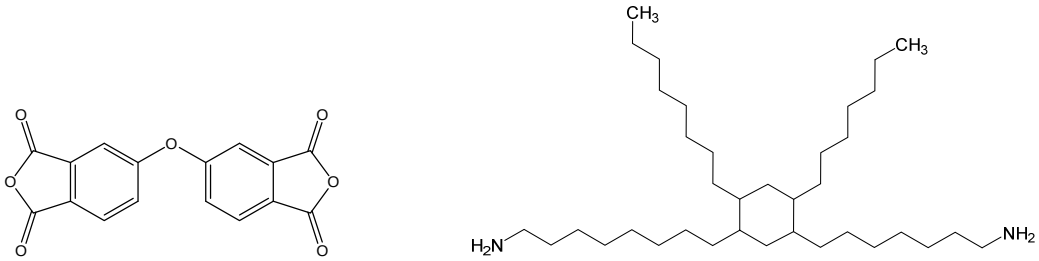


**Scheme 1.** Idealized structures of the monomers used in the SH-PEI synthesis. Left shows 4,4'-oxydiphthalic anhydride (4,4'-ODPA) and right shows a generalized structure of the dimer diamine (DD1).

*1st step: Polyamic acid synthesis (PAA)*

The diamine is weighed and dissolved in 9/10 (vol.) of the solvent (DMAc) in a three neck round bottom flask. The dianhydride is then added to the flask with the help of a funnel rinsed by the rest of the solvent (1/10 (vol.)). The mixture is then magnetically stirred at 200 rpm under nitrogen flow at room temperature and left to react until the solids are dissolved and the solution appears clear and light yellow suggesting the formation of the polyamic acid, PAA (Scheme 2). The monomers conversion and PAA formation was controlled by ATR-FTIR (Figure S1, SI).

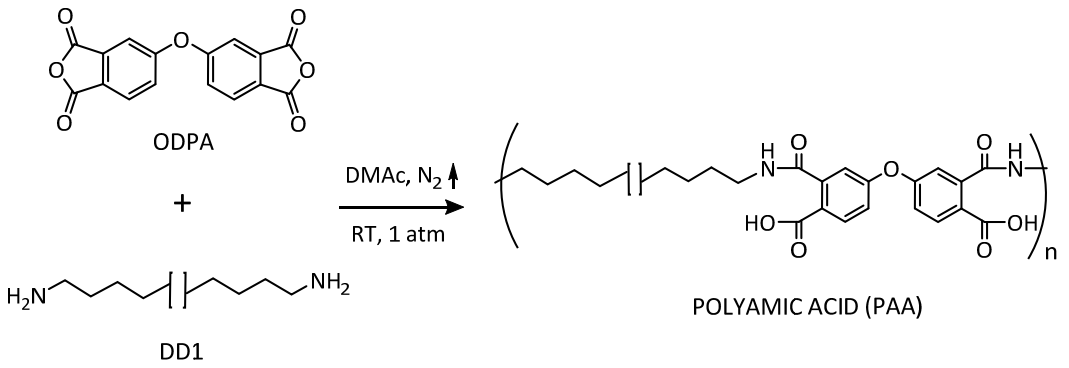


**Scheme 2.** Schematic representation of the polyamic acid synthesis. DD1 structure is shown in a simplified way where the brackets refer to the branched section, which can be positioned at different places along the main C18 chain.

*2nd step: Thermal imidization in solution (PEI)*

The thermal cyclodehydration in solution was used to form the bulk polyetherimides (Scheme 3). For this the three neck round bottom flask containing the prepared polyamic acid solution is attached to the 10 mL Dean-Stark apparatus with a reflux condenser in order to perform the azeotropic distillation. After stirring under nitrogen flow at 150 rpm for 6 hours at 155°C and 1 atm the aqueous phase was removed in a Dean-Stark trap by azeotropic distillation with 10 vol% toluene as an azeotrope.

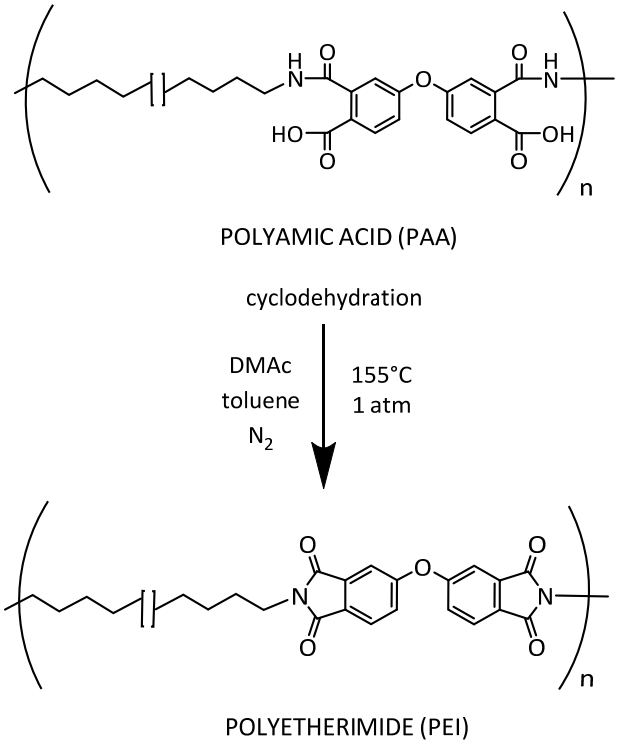


**Scheme 3.** Schematic representation of the thermal imidization reaction in case of stoichiometric reaction (cyclodehydration of polyamic acid into a polyetherimide).

The solution is then left to cool down overnight. Upon cooling down to room temperature, a very viscous/rubbery polyimide product is obtained at the bottom of the flask. The remaining DMAc is then poured off and the polymer is transferred from the flask to a glass tray and put to dry in a vacuum oven for 2 hours at 80°C, 1 hour at 120°C and 1 hour at 200°C. Cooling down to room temperature is done in vacuum as well. The glass tray with the thick polyimide film is then soaked in lukewarm water (~40°C) overnight. Upon drying at room temperature, the polyimide film is peeled off from the substrate and stored in a desiccator partially filled

with dry silica gel. The films are then manually granulated and re-shaped in a dog-bone-shaped PTFE mold with dimensions according to ASTM D1708 (length, l=22 mm; width, w=5 mm; thickness, t=2±0.3 mm). Once in the mold the samples were brought to a post-treatment in a vacuum oven at 150 °C for 11h followed by 1h at the atmospheric pressure. After heating the samples were allowed to cool down in air to room temperature overnight. This led to the bulk polyimide samples necessary to evaluate the generic properties and healing.

## 2.2. Characterization methods

*2.2.1. Infrared spectroscopy*

Attenuated Total Reflectance Fourier Transform Infrared (ATR-FTIR) spectroscopy was employed in order to follow reaction completion and detect possible unreacted groups influencing the healing process at freshly cut surfaces. Each IR spectrum was recorded as an average of 3 scans in the wavenumber range 4000-500 $cm^{-1}$. The scans were performed at the newly created surfaces immediately after manually cutting the bulk sample with a razor blade.

*2.2.2. Gel permeation chromatography*

Molecular weight distributions of synthesized polymers were determined by gel permeation chromatography (GPC) using polystyrene as the standard. Polymer solutions were prepared in tetrahydrofuran (THF), concentrations 1 mg/mL.

*2.2.3. Thermal analysis*

Thermal properties were evaluated by thermogravimetric analysis (TGA) and differential scanning calorimetry (DSC). All measurements were performed under nitrogen. TGA was run from room temperature to 595°C at 10°C/min. DSC measurements were carried out at 10°C/min following this procedure: (1) heating from -50°C to 200°C; (2) maintaining for 2 min at 200°C; (3) cooling down to -50°C and (4) repeat steps 1 to 3. The glass transition temperature ($T_g$) was determined from the second heating cycle. No crystallization nor melting peaks were detected in any of the samples in the tested temperature range.

*2.2.4. Density determination*

The density of the polymers was determined by hydrostatic weighing method coupled with an analytical laboratory scale with a precision of 0.1 mg.

*2.2.5. Tensile properties and interfacial healing evaluation*

Tensile mechanical tests were performed using dog-bone specimens according to the ASTM D1708 standard (thicknesses, t=2±0.3 mm) at 80 mm/min crosshead speed. To determine the healing behavior, pristine samples were cut with a sharp razor blade at room temperature. After cutting, the two broken pieces were carefully repositioned in the dog-bone PTFE mold and allowed to heal at the required temperature with around 40% RH for 1, 5 and 11 days. For each polymer composition, three samples were tested in the pristine state and three samples in the healed state. The healing efficiency was calculated based on the following equation:

$$Healing\ efficiency\ (\%) = \frac{\sigma_b^{healed}}{\sigma_b^{pristine}} \times 100 \qquad \text{Eq. 1}$$

where $\sigma_b^{healed}$ and $\sigma_b^{pristine}$ are the stress at break for healed and pristine samples, respectively.

*2.2.6. Rheological measurements*

The linear viscoelastic properties of SH PEIs were investigated by the Haake Mars III rheometer, using the parallel plate geometry, with plate diameter of 8 mm. Preliminary strain amplitude sweeps at 1 Hz were performed at the highest and the lowest tested temperatures, from 0.001% to 10% strain to determine the linear viscoelastic region for the different polymers. Based on these results, a shear strain amplitude of 0.04% for **D-1.2** and 0.5% for the other three polymers was used to ensure the tests were performed in the linear viscoelastic region. Frequency sweep experiments from 10 to 0.1 Hz were performed at temperatures between 110 and 10 °C, in steps of 5 °C. The rheological mastercurves at the reference temperature of 25 °C were constructed from the obtained data applying the time-temperature superposition principle (TTS) using the dedicated Rheowin software. Each polymer was tested twice showing high reproducibility.

## 3. Results and discussion

### 3.1. Effect of ODPA/DD1 ratio on the branched-PEI architecture and properties

The conversion of monomers to PAA and subsequent imidization of PAA to PEI was monitored by FTIR as shown in Figure 1 for D-1.1. The imidization of PAA into PEI can be confirmed by the disappearance of the amic acid peaks typically visible at 1716, 1640 and 1550 $cm^{-1}$ in PAA spectra and the appearance of the characteristic peaks of imide bonds at 1770, 1710, 1360 and 745 $cm^{-1}$ in PEI spectra. The imidization reaction was confirmed for all the polymers (Figure S1, SI) and supported by $^{1}H$ NMR analysis (Figure S3, SI). The percent yields were calculated by the standard approach shown in SI (Page S-2). Yields of 45% for D-0.9, 89% for D-1.0, 85% for D-1.1, 93% for D-1.2 were obtained. The lower yield obtained in the case of the excess of ODPA system is in line with other reports on polyimide synthesis with an excess of dianhydride (25).

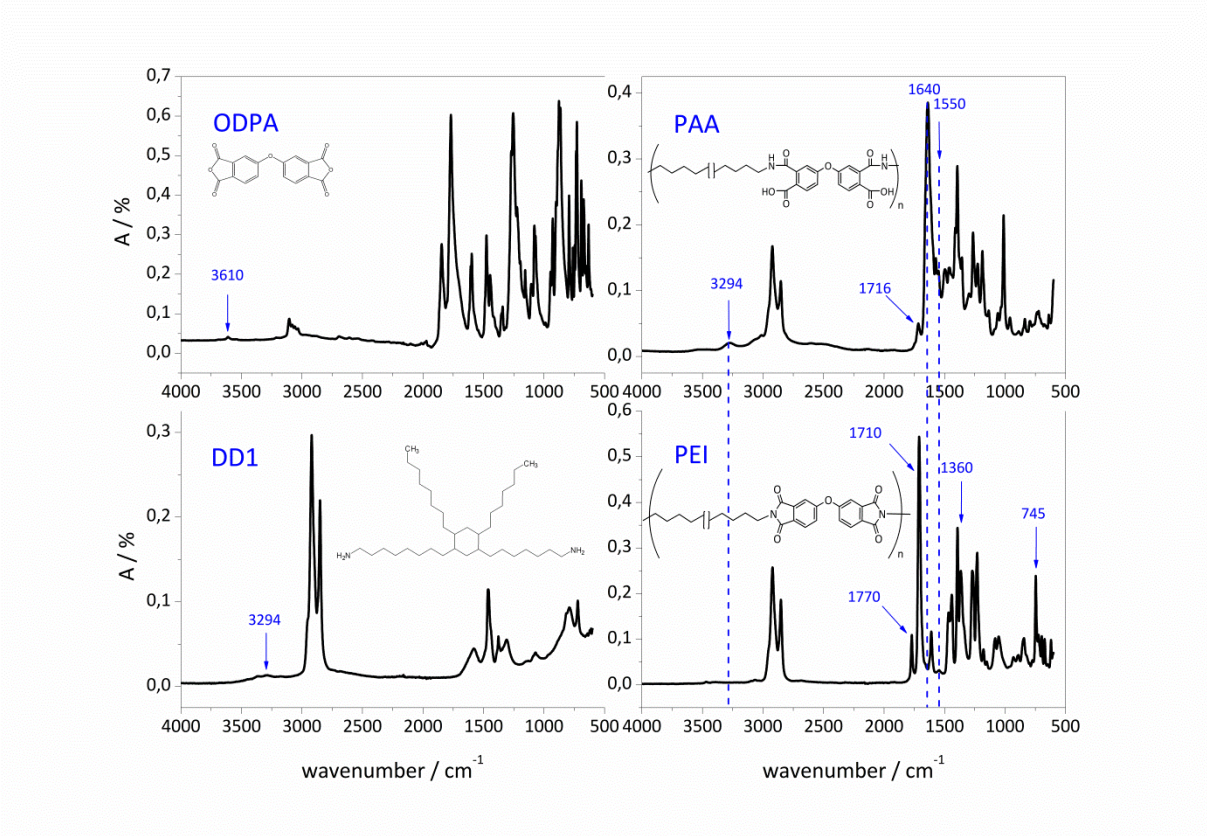


**Figure 1.** IR spectra of monomers ODPA and DD1 (left), prepolymer PAA and polymer PEI of sample D-1.1 (right). Figure shows the conversion of monomers into PAA and imidization of PAA into PEI.

The resulting polymers were then analyzed by GPC and the relevant information is presented in Table I. The results show that the synthesis led to polymers with a normal polydispersity that increases with DD1 content.

Polymers D-1.0 and D-1.1 show a $M_w$ twice that of the D-0.9. No information is shown for D-1.2 because, as opposed to the other three polymers, this sample was swelling but not soluble in any of the solvents tested in this work (toluene, chloroform and THF) suggesting its partial crosslinking.

**Table I**. Effect of the DD1 content (i.e. offset from theoretical stoichiometric ratio) on $M_w$, $M_n$ and PDI as calculated from the major peak obtained in GPC. Tg obtained from DSC and temperatures for 2% weight loss obtained from TGA.

| Polymer | $M_w$ (g/mol) | $M_n$ (g/mol) | PDI | DSC-$T_g$ ($^oC$) | TGA-T (2% wt. loss) (°C) | Density ($g/cm^3$) |
|---|---|---|---|---|---|---|
| **D-0.9** | 18k | 11k | 1.6 | 17 | 360 | 1.06 |
| **D-1.0** | 32k | 16k | 2.0 | 13 | 380 | 1.05 |
| **D-1.1** | 35k | 15k | 2.3 | 8 | 400 | 1.04 |
| **D-1.2** | * | * | * | 5 | 360 | 0.98 |

* GPC data not available since D-1.2 is not soluble in the GPC solvents available.

The effect of the ODPA/DD1 ratio on the branched-PEI polymer architecture was further confirmed by a detailed FTIR analysis of the freshly cut polymer surfaces as shown in Figure 2 for selected regions of interest (full IR spectra can be seen in support information, SI, Figure S1). Figure 2a shows a presence of the peak at 3670 $cm^{-1}$ for the sample D-0.9, which is not present in the other samples. This peak, corresponding to free -OH groups, can be associated to the presence of –COOH terminated chains produced due to the excess of dianhydride as proposed in Scheme 4a. On the other hand, the IR spectrum of polymer D-1.2 shows the presence of a broad peak in the region 3400-3280 $cm^{-1}$ and two peaks at 1660 and 1540 $cm^{-1}$, this being an indication of the formation of mono-substituted amides during chemical crosslinking and formation of a polyimide-amide network (26) as shown in Scheme 4b. These results confirm that the maximal polymer chain length is obtained for compositions close to the stoichiometric ratio. However, when a certain amount of diamine surpasses a critical limit chemical crosslinks are promoted and chain formation is reduced. WAXS and SAXS (Figures S2a and S2b, SI) further showed the absence of crystallinity, ordered regions, and phase separation thereby confirming the amorphousness and homogeneity of all the polymers.

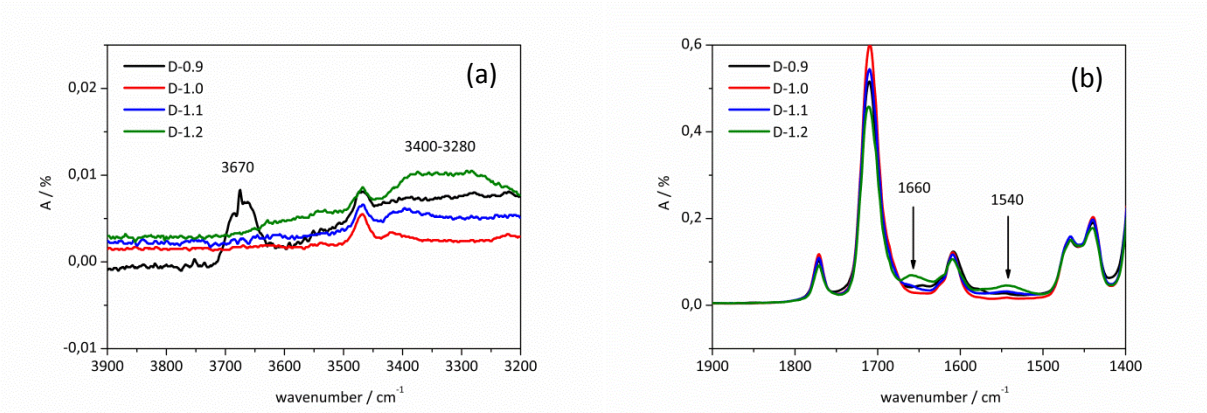


**Figure 2.** Magnified IR spectra of the regions of interest for the SH-PEI polymers as a function of the offset from the theoretical stoichiometric ratio. **a)** free -OH groups in D-0.9 and -NH stretch for D-1.2; **b)** amide II bands in D-1.2. Full spectra can be seen in Figure S1, SI.

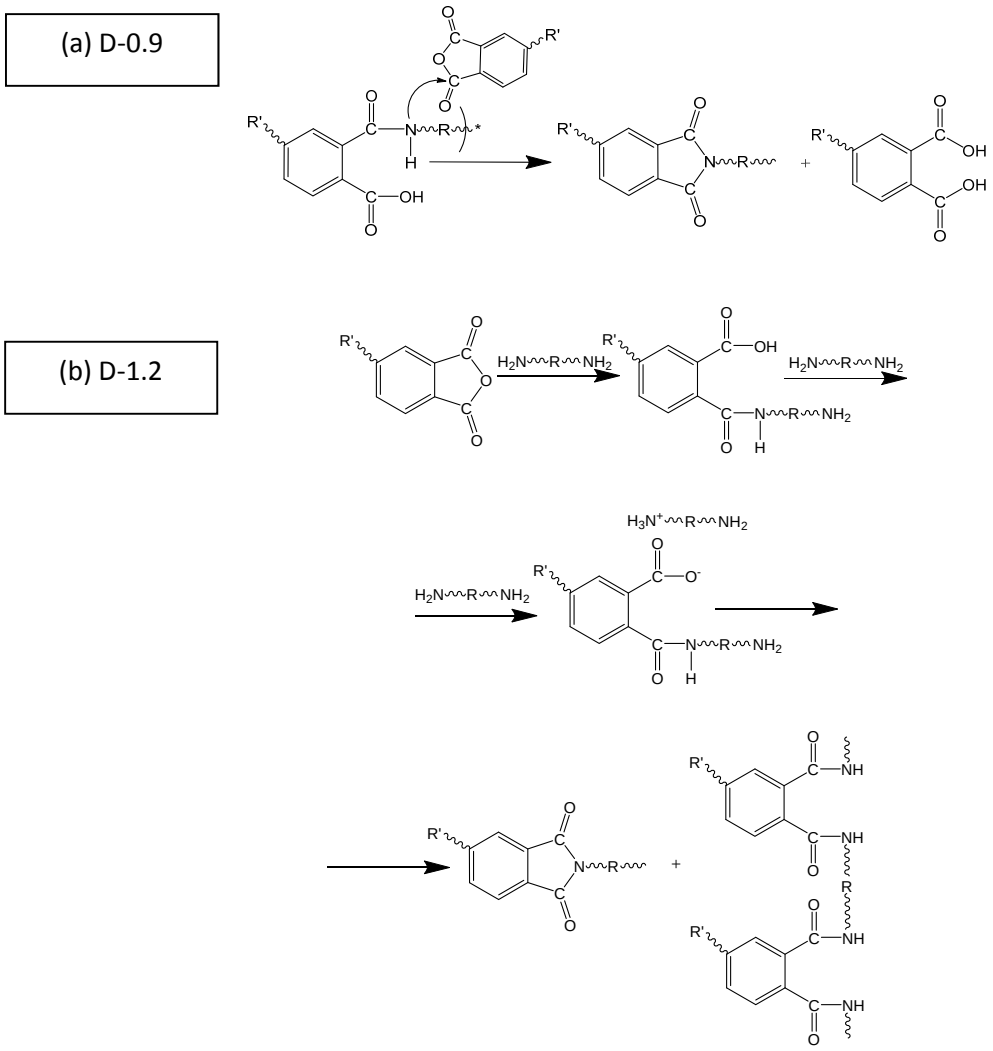


**Scheme 4.** Schematic representation of the effect of the excess **(a)** dianhydride; **(b)** diamine during imidization reaction. DD1 structure is simplified.

The effect of the polymer architecture on the thermal and mechanical behavior was further studied by TGA, DSC and tensile testing. All polymers show a high thermal stability independent of their architecture with values for the onset degradation temperature (2% weight loss) at around 400°C (Table I) similar to those of traditional commercial polyimides such as LaRC-IA. Furthermore, all samples (Figure S5, SI) showed only a small weight loss up to 0.4% until 200 °C suggesting that almost no solvent (toluene or DMAc) was entrapped during the imidization and that the monomers were fully reacted. It should be noted that samples D-0.9 and D-1.2 show slightly lower degradation onset temperatures probably due to the lower $M_w$ of D-0.9 and the presence of more thermally sensitive amide linkages in the case of D-1.2 (27). DSC shows that higher DD1 contents lower the $T_g$ of the polymers from 17 °C to 5 °C (Table I), but did not show any melting nor crystallization peaks in agreement with XRD results. Such a decrease in $T_g$, even for the crosslinked polymer, can be justified by a local plasticizing effect of the dangling chains according to the "iso-free volume" hypothesis and the "tent-pole-effect" (28). In line with this, the apparent density was found to decrease linearly with the DD1 increase although D-1.2 appears as an outlier to the trend (Table I). This trend is in agreement with previous reports showing that the large van der Waals radii of branching points can sterically hinder the charge transfer complexes formation in aromatic polymers (e.g. polyimides) thereby leading to a higher free volume due to a chain packing decrease (29). The outlier behavior of D-1.2 can be related to the presence of bulky DD1 groups as cross-linkers between chains in a partially crosslinked network, thereby reducing the chain packing density significantly more than the expected effect of more DD1 in a linear polymer. The promotion of chemical crosslinking with the DD1 increase was further confirmed by a swelling test, as shown in the supporting information, Table S-I.

Figure 3 shows the strain-stress curves of the four polymers (detailed characteristic parameters can be seen in Supporting Information, Table S-II). All polymers exhibit rather high values for fracture stress and strain at break. The ultimate tensile strength decreases with DD1 content which can be explained by a gradual increase in the amount of amide bonds formed instead of the stronger imide bonds preferentially formed below and at the theoretical optimal stoichiometric ratio. However, the strain at break follows a clear trend from D-0.9 to D-1.1 increasing with the amount of branched DD1 units. This trend is not followed when the DD1 excess reaches 20 mol.% (D-1.2). At this point, the amide crosslinks formed do not allow the network to stretch as much as the DD1 content would predict thereby reducing the elongation at break.

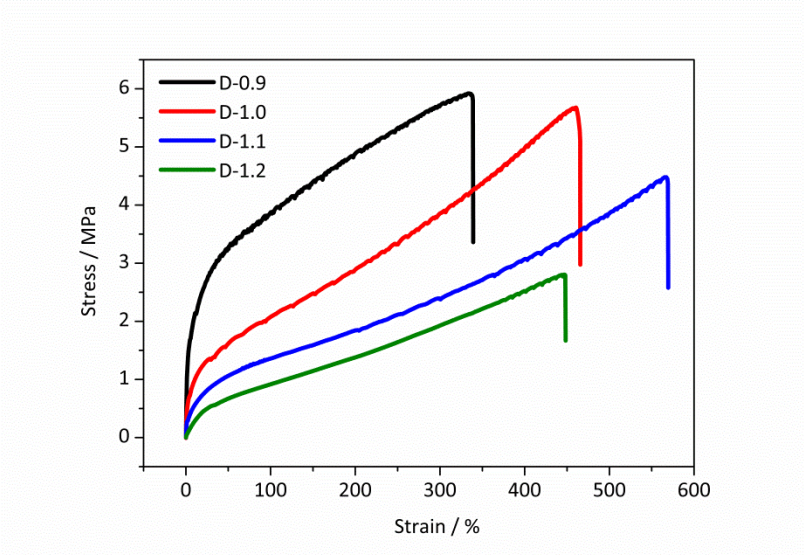


**Figure 3**. Stress-strain curves at 80 mm/min strain rate showing the effect of the DD1/OPDA ratio on the general mechanical performance.

In order to obtain a deeper understanding of the branching effect on the dynamic behavior of the polymer, frequency sweep rheology in parallel-plate geometry was performed for its potential to discriminate dynamic behaviors at different time scales (30). In order to be able to analyze a broad frequency range beyond the experimental practical limits the time-temperature superposition (TTS) approach was employed. It should be noted that the TTS is in principle applicable only to polymers that are thermo-rheologically simple. Typically, copolymers, polymer blends, or polymers with strong secondary supramolecular interactions show difficulties in obtaining a good superposition. However, previous studies show that in certain thermo-rheologically complex polymers, TTS might still be a useful and valid tool at certain temperature and frequency regimes (31). In this study, we found that TTS is applicable to these polyetherimides within the frequency range of interest ($10^{-7}$< f <$10^{5}$ Hz). The mastercurves of the elastic modulus (G'), viscous modulus (G'') and tan δ shifted to a reference temperature of 25 °C (healing T) are shown in Figure 4 while the most relevant parameters obtained from the rheological tests are listed in Table II. Shift factors plotted versus inverse temperature can be found in the Figure S6b, SI).

From an initial analysis it can be observed that the obtained mastercurves for the different PEIs resemble the ones of lightly entangled polymers (32, 33) with four polymer-state regions identified by the intersection points between G' and G", as shown in Figure 4 for the polymer D-1.0 and reported in Table II:

(i) $f > f_g$ : Glassy regime (G’ > G”) where the network is frozen and chain movements are restricted;

(ii) $f_d < f < f_g$ : Dissipative regime (G” > G’);

(iii) $f_s < f < f_d$ : Apparent elastic plateau (G’ > G”);

(iv) $f < f_s$ : Viscous flow (G” > G’).

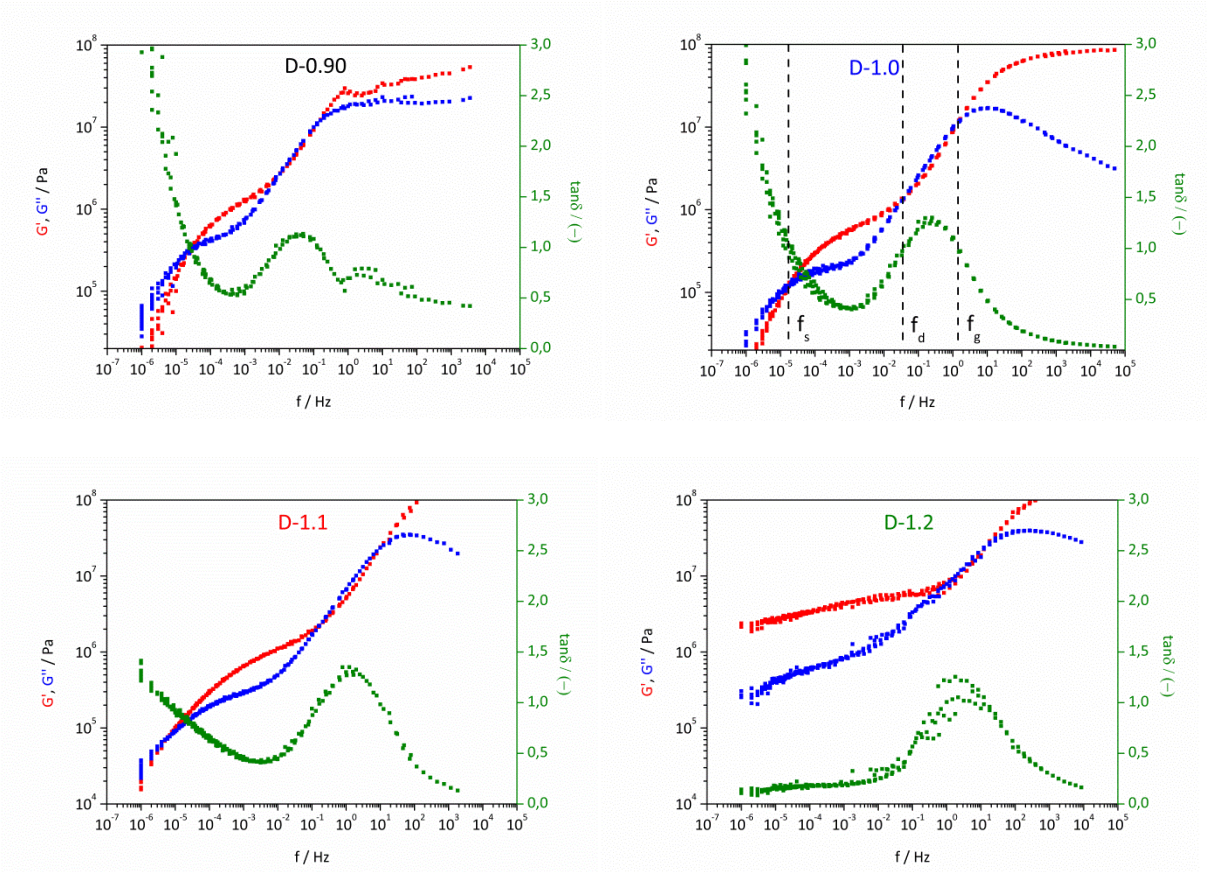


**Figure 4.** TTS mastercurves at $T_{ref}$ = 25 °C. Storage modulus (G’, red symbols), loss modulus (G’’, blue symbols) and loss tangent (tanδ, green symbols) as a function of shifted frequency ($a_T$·f) for four different PEIs with respect to the stoichiometric offset.

**Table II**. Characteristic parameters obtained from rheology.

| Polymer | $f_s$ (Hz) | $f_d$ (Hz) | $f_g$ (Hz) | $\tau_s$ (s) | $\tau_d$ (s) | $\tau_g$ (s) | G' slope at $f<f_s$ | G" slope at $f<f_s$ | $G_N$* (Pa) | $M_e$** (g/mol) |
|---|---|---|---|---|---|---|---|---|---|---|
| **D-0.9** | $2.6\cdot10^{-5}$ | 0.011 | 0.14 | $3.8\cdot10^{4}$ | 91 | 7.1 | 1.63 | 0.95 | $1.25\cdot10^{6}$ | *2100* |
| **D-1.0** | $2.0\cdot10^{-5}$ | 0.035 | 1.5 | $5.0\cdot10^{4}$ | 28 | 0.7 | 1.25 | 0.83 | $6.09\cdot10^{5}$ | *4270* |
| **D-1.1** | $5.2\cdot10^{-6}$ | 0.180 | 10 | $1.9\cdot10^{5}$ | 5.5 | 0.1 | 0.73 | 0.58 | $9.21\cdot10^{5}$ | *2800* |
| **D-1.2** | - | 1.500 | >10 | - | 0.7 | < 0.1 | 0.09 | 0.16 | ($1.62\cdot10^{6}$) | 1500 ($M_c$) |

* $G_N$ calculated from the van Gurp-Palmen plot, δ(|G|*), (Figure S6a, SI) (34, 35); with exception of D-1.2 where the minimum G' value from the mastercurve is used.

**$M_e$ were calculated according to $M_e = \rho RT/G_N$ (Doi and Edwards) equation, using experimentally determined densities (Table I). $M_e$ values must be considered as pseudo-$M_e$ values governed by 'transient interactions' not as molecular weight between entanglements, while $M_c$ value for D-1.2 are related to the permanent crosslinks present in this polymer grade.

The rheology plots are also similar to those reported for supramolecular polymers. In supramolecular polymers, the lowest frequency crossover is usually associated to the relaxation of the supramolecular or secondary interactions. Above this crossover, the supramolecular crosslinks or constraints are intact and the network is in its closed state. Below this frequency ($f < f_s$), the network is said to be in terminal flow region (G">G') and the network is in its open state. As expected, this crossover is seen for all the polymers except for D-1.2 which further confirms the presence of a permanently crosslinked network in this polymer (36). Moreover, several studies have shown that polymers with supramolecular or transient interactions have two relaxation plateaus for the elastic modulus (37, 38). Following this, in the polyimides studied in this work, which show multiple relaxations, the plateau at intermediate frequencies ($f_s < f < f_d$) could be attributed to transient constraints. As seen in Table II, the plateau moduli ($G_N$) for these polyimides are of the order of $10^5$-$10^6$ Pa. Such values are in agreement with similar values obtained for supramolecular self-healing polymers based on metal ionic interactions in rubbery poly(n-butyl acrylate) ionomers (39), hydrogen bonding end groups in poly(isobutylene) (40) and ionic networks reacting neutralized citric acid and aliphatic diamines (41). When the relation of rubber

elasticity, $G_N = \rho RT/M_e$, is applied to these polymers and the molecular weight between effective interactions $M_e$ is calculated, values of $M_e$ between 2000 and 4000 g/mol are obtained (Table II). These values seem to be lower than the minimum possible entanglement molecular weight for polymers (42), which suggests that the rubbery plateau is not governed by chain entanglements but by other type of interactions. Based on the architecture of these polymers with a high branching density we propose that the apparent elastic plateau is governed by secondary but numerous van der Waals interactions between the dangling chains, where apparent entanglements must be given by branching and interchain interactions. This interpretation is nevertheless not applicable to the sample D-1.2. In the latter case the plateau is related to its crosslinking nature and $M_e$ can be interpreted as molecular weight between crosslinks ($M_c$). Swelling tests confirmed the crosslinking nature of D-1.2 leading to $M_c$ values of 929 ± 14 g/mol.

A detailed analysis of the slopes of G' and G'' in the dissipative ($f_d < f < f_g$) and terminal relaxation ($f < f_s$) regions also gave relevant information related to the dynamic interactions within the polymer (Table II). Generally, for polymers showing true terminal relaxation the slope of G' is 2 and that of G" is 1, which fits the well-known Maxwell model for polymers (43). The PEIs here investigated show slope values in the terminal relaxation region ($f < f_s$) lower than 2 and 1 which at the same time decrease with the amount of branched DD1 (Table II). On the other hand, the slopes of G' and G'' at the dissipative region ($f_d < f < f_g$) are equal to 0.5. In previous works on supramolecular polymers have related slope values similar to those in the dissipative region of our polymers to the presence of multiple supramolecular stickers (44) hindering chain reptation, while the strength and number of the supramolecular stickers make the terminal relaxation to follow sticky Rouse-like or constrained dynamics (30, 45-47). Based on this it seems reasonable to state that the slope values here obtained also give an indication of secondary interactions affecting chain dynamics. The most likely explanation is therefore that the aliphatic branches act as stickers controlling the molecular motion of polymer main chains. Interestingly, in the dissipative region no differences in the slopes are observed while the relaxation time constants $\tau_g$ and $\tau_d$ decrease with the increase in DD1. Such observation indicates that these motions occur at shorter time constants for the polymer with the highest DD1 content but once they are taking place, the kinetics of motion is the same. Contrary to this effect, the motions at low frequencies (high times) seem to initiate later in time for D-1.1 (higher $\tau_s$) and once in operation these motions occur at lower kinetics than in D-0.9 and D-1.0. Based on these results and the polymer architecture we propose that the first dissipative

motions are related to dangling chain interactions governed by $T_g$ while motions at low frequencies correlate to long range chain motions (i.e. reptation or interdiffusion) highly restricted by the dangling chains where the more the dangling branches (higher DD1 content) the higher the restriction to motion (i.e. D-1.1 is more restricted than D-0.9).

Four idealized polymer architectures of the amorphous branched thermoplastic elastomeric PEIs can be sketched as shown in Figure 5: low molecular weight polymer with near RT Tg (D-0.9), two systems with similar Mw but different $T_g$ (D-1.0 and D-1.1), and a partially crosslinked branched polyamide-imide (D-1.2). This set of samples allowed for a detailed study of the effect of the architecture on the healing properties of these new room temperature healing polymers as shown in the next sections.

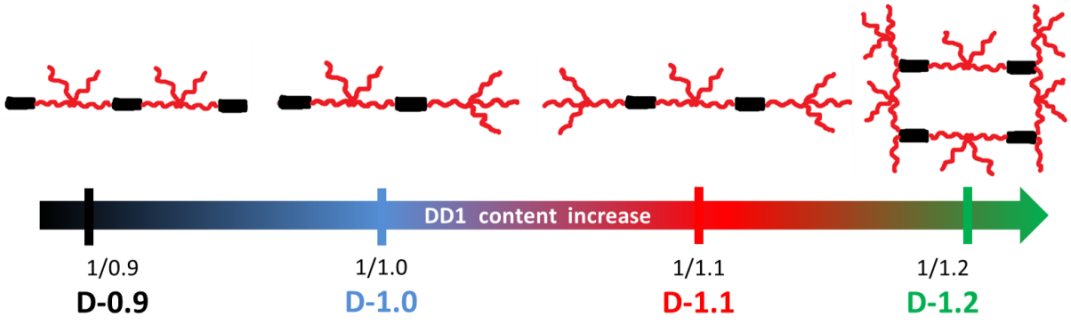


**Figure 5.** Sketch depicting the effect of the ODPA/DD1 offset ratio on the PEI polymer architecture.

### 3.2. Effect of the polymer architecture on the room temperature healing

Figure 6 shows the representative healing results of the developed PEIs obtained for samples tested in tension as function of the healing time and DD1/ODPA ratio at room temperature (23±2°C). From this figure, it becomes evident that near 100% healing efficiency can be obtained with both D-1.0 and D-1.1 samples in the time studied. Nevertheless, there is a significant difference between these two with respect to the healing kinetics. While D-1.1 achieves apparent maximum healing somewhere between 1 and 5 days, D-1.0 maximum healing occurs somewhere between 5 and 11 days. The sample with the lowest and the highest DD1 content (D-0.9 and D-1.2) show no significant healing in the investigated time and healing temperature. It is worth mentioning that all the samples fractured at the healed interface for healing times up to 11 days.

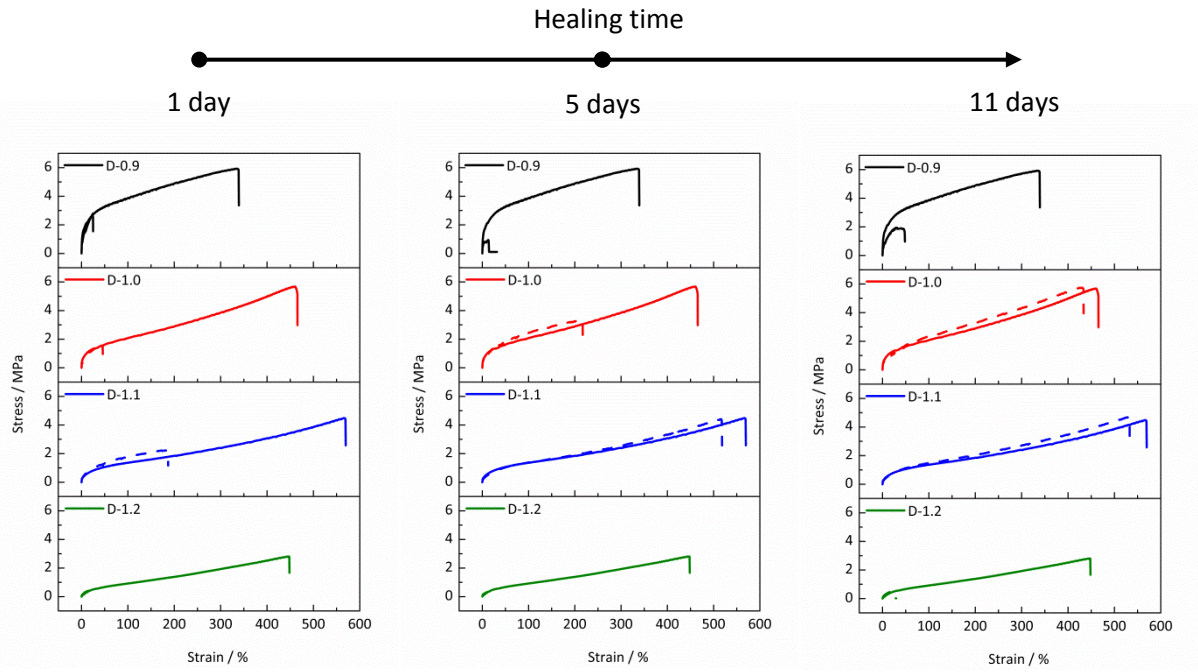


**Figure 6.** Stress-strain curves showing the PEIs healing behavior at the room temperature as function of the stoichiometric offset and healing time. Full lines represent pristine (—) and dashed lines represent healed (---) samples.

However, when D-1.0 and D-1.1 samples were given 30 days to heal, fracture always took place far away from the healed original fracture plane (Figure 7). This demonstrates that the original fracture plane is no longer the weak part of the specimen and strength has recovered.

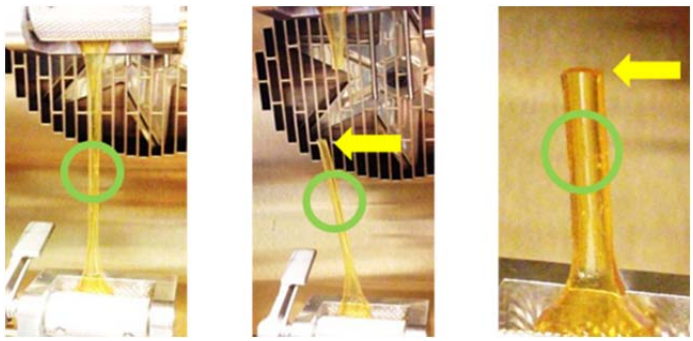

**Figure 7.** Captures from a video showing the D-1.1 sample breaking away from the healed spot after 30 days of healing at RT. The green circle points out the healed location.

In contrast, the two grades D-0.9 and D-1.2 still showed fracture at the healed interface region even after 30 days. Based on these results a three-stage healing process at the macroscale can be suggested as shown in Figure 8.

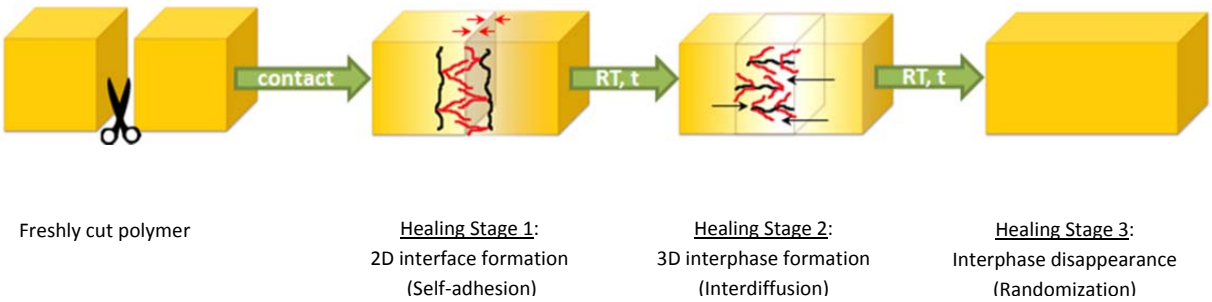


**Figure 8.** Sketch depicting the stages of the SH PEI healing process.

This full process is more clearly seen for samples D-1.0 and D-1.1. During the first healing stage, an adhesive process leading to weak interfacial restoration takes place (visible in D-0.9, D-1.0, D-1.1 and in a lower degree D-1.2 at short times). The length of the initial stage shortens as the DD1 content increases as can be seen in Figure 6. As long as contact time advances interfacial wetting increases and a second stage takes place in the D-1.0 and D-1.1 samples. This second stage allows the transition from an interface phenomenon (surface contact) into an interphase formation (volume involved in the healing) most likely due to chain interdiffusion. The absence of the last two stages in polymer D-1.2 can be explained by its crosslinked nature that only allows some interfacial initial adhesion. The transition of an interface into an interphase failure can be detected in mechanical fracture testing by the failure mode transition switching from adhesive failure to cohesive failure with deformation at the damaged zone before failure (48, 49). Again, detailed SAXS measurements did not show any sign of formation of new local microstructures upon extensive healing.

### 3.3. Relationship between polymer architecture and healing

When relating the rheological results to the macroscopic healing behaviour and the general polymer architecture, several correlations emerge. The first observation is that an excess of DD1 leading to a partially crosslinked network leads to a non-healing material irrespective of the testing temperatures and times. Contrary to this, the other three samples show a strong time-dependency of healing with no healing for D-0.9 at room temperature.

We and other research groups have related the dynamics of reversible self-healing to the supramolecular bond lifetime ($\tau_b$). $\tau_b$ values between 10 s and 100 s are claimed to lead to a combination of healing in reasonable times and decent mechanical properties (39). Nevertheless, in the present work, the $\tau_b$ principle was not applicable as three crossovers interplay and affect healing as shown in section 3.1. A different approach was therefore here used to characterize and understand the behavior of this new type of room-temperature self-healing polymers with complex behavior.

In Figure 6 faster healing is observed for the sample D-1.1 while the rheological data in Figure 4 suggests that healing should be faster for sample D-0.9 as this one has lower $\tau_s$ and higher slope (kinetics of the motion are faster). The first thing to note here is that the TTS principle typically loses validity when multiple molecular motion mechanisms play a role and the polymer system is more temperature sensitive. In our case the higher the DD1 the more temperature sensitive the network is and therefore the TTS approach loses theoretical validity at higher frequencies, affecting mainly the calculated $\tau_s$ values (the G' and G'' slopes are not affected). Despite the absolute $\tau_s$ values could therefore be inaccurate we believe the trend and slopes would not be highly influenced and the conclusion would remain the same. The second remarkable point is that the dynamics at short times occur faster in the case of D-1.1. When looking at the times at which the motions occur and compare the values to the obtained macroscopic healing times (i.e. tensile) it can be found that at the tested times all the motions should have started at least for the 5 days testing (as $\tau_s$ < 2 days according to rheology). What can be seen in the macroscopic healing is that, at these testing times, only the D-1.1 sample has reached maximum healing while D-0.9 still shows low healing. This observation suggests that healing is in this case controlled by another factor. The nature of this additional factor can be found in the dissipative region observed in rheology. High contents of branching with no crosslinking (D-1.1 and D-1.0) show dissipative motions occurring earlier in time ($\tau_g$ smaller) but also reach the plateau earlier in time ($\tau_d$ smaller) than D-0.9

which makes that the three polymers can show similar initial sticking and rubbery behavior in the mechanical testing. This can be seen in the short-term macroscopic healing tests for which all three samples show sticking seen as small mechanical recovery (at 1-day healing test). After reaching this point the chains should be able to interdiffuse in order to lead to full healing but for this to occur it is necessary that the temperature of healing is significantly higher than the $T_g$ (else the necessary condition of chain motion will not be met). This last condition is certain for D-1.1 but not for D-1.0 and D-0.9. In order to prove this hypothesis we healed D-0.9 at a higher temperature than room temperature ($T_g$ + 12 °C = 29 °C) and tested it at room temperature. The results shown in Figure S7 (SI) show a faster healing than for D-1.1 reaching a maximum ~75% healing already at 1-day healing time thereby proving our hypothesis.

To confirm the effect of the branches on healing, a comparable PEI with no alkyl-dangling branches was synthesized by replacing the DD1 with a linear C12 aliphatic diamine (1, 12-diaminododecane) at theoretical stoichiometric ratio with the same dianhydride, ODPA. This non-branched polymer is expected to have more dense chain packing, partially due to charge transfer interactions as the aromatic groups are not hindered by bulky alkyl chains (7, 31). As shown in Table S3 in SI, this sample (ND-1.0) showed a significant increase in the $T_g$ (69 °C) but showed no healing even upon heating up to temperatures as high as 90 °C. As can be seen in the TTS mastercurve, in Figure S8a (SI), the relaxation transitions appear at much lower frequencies than for its branched counterpart. Furthermore, the non-branched polymer shows the appearance of a marked rubbery plateau thereby confirming the effect of the branches on the global polymer dynamics and their role on healing.

When unravelling the effect of the branches on healing and relating rheology to macroscopic healing it is also relevant to compare the results found in this work to other reported comparable self-healing supramolecular polymers. On the one hand some authors have used branched aliphatic monomers similar to DD1 to create supramolecular networks although in their work they included secondary ionic interactions (21). Such polymers showed a lack of terminal flow zone for certain network compositions as in our case, but it was attributed to block-like ordering in the network promoted by the ionic interactions and verified using calorimetric analysis showing a second thermal transition referred to as the order-disorder transition temperature. On the other hand, Chen et al. (50) presented self-healing branched polymers but reported that healing was related to phase

separation-induced order-disorder. However, none of the previously reported works presented a concept similar to the one here introduced where healing is dominated by alkyl chains with no phase separation nor reversible covalent or strong non-covalent interactions. To prove this concept more dedicated tests were performed. To show the potential elastic contribution of the DD1 to healing, rheological temperature sweeps were performed for the liquid branched dimer diamine DD1 used in this work (Figure S9, SI). The results revealed its elastic behavior up to a temperature of 40 °C, analogous to the non-Newtonian behavior in structured fluids, which was also noticed before by Aboudzadeh et al. (21). This elastic nature hints towards the presence of attractive interactions between the alkyl groups of the dangling branches forming some kind of chain ordering such as micro phase-separation (50). However, small angle X-ray scattering (SAXS) tests (Figure S4b, SI) did not provide evidence of any phase separated ordering or block-like structure in the domain size range of 5-100 nm. DSC results also showed no thermal transition other than $T_g$, thus confirming completely amorphous polymers without structural ordering. It should also be noted that, based on the monomers an spectroscopic analysis, it is safe to say that there are no other chemical functionalities in these polymers that can lead to hydrogen-bonding or ionic interactions and that the charge transfer complexes formation is hindered by the bulky branches. Hence based on the rheological observations, we can conclude that the weak but numerous van der Waals interactions between the alkyl groups of the dangling branches of the aliphatic diamine create a transient supramolecular network which makes these polymers mechanically robust yet self-healing. This is the first time, to the best of our knowledge, that a self-healing polymer based on this principle is presented. Furthermore, the combination of healing at room temperature and the relatively high values of the mechanical properties obtained for the best performing polyimides reported here is, to the best of our knowledge, unique. The (room temperature) Young modulus values of the polyimides presented here are in the range from 30 to 110 MPa. These values are up to two orders of magnitude higher than the values reported for other elastomers healing at room temperature, such as the ones based on H-bonds (E~0.25 MPa) (19), those based on the combination of H-bonds and aromatic disulfides (E~0.10 MPa) (51) or the H-bonds multiphase brush polymers from Chen et al ($10 < E < 40$ MPa) (50). Intrinsic self-healing polymers with higher modulus exist, but these require temperatures well above room temperature for healing. Our inability to compare the healing performance of polymers in an objective and quantitative manner stems from the multi-dimensional nature of the issue and the absence of accepted testing protocols (52).

## 4. Conclusions

New room temperature healing semi-aromatic thermoplastic elastomer polyetherimides based on aliphatic branched dimer diamine were synthesized and fully characterized. The polymers show remarkable healing behavior at room temperature combined with mechanical properties close to application relevance. General polymer properties and healing efficiency were found to be dependent on the branched diamine content for which an optimum value was found. High contents of branched diamine led to disabling the macroscopic healing due to partial crosslinking reactions. On the other hand low branching led to the decrease of the healing kinetics. A dedicated macroscopic healing kinetics study combined with a frequency sweep rheology analysis for both linear and branched polymers confirmed the role of the aliphatic branches on the healing mechanism and kinetics. The proposed healing mechanism is based on a two-step process with fast van der Waals interactions between dangling aliphatic chains forming a 2D interface followed by a second slower step where chain interdiffusion leads to a 3D interphase formation. Provided sufficient equilibration time, the interphase disappears leading to the full restoration of polymer properties. Even though similar branched dimer building blocks were used before in self-healing polymers, this is the first time, to the best of our knowledge, that the healing was obtained without thermo-reversible bonds or supramolecular interactions (hydrogen, ionic, etc.) other than van der Waals. Although the concept has been proven for polyimides it is believed that introducing long aliphatic branched monomers into a robust polymer backbone can lead to high mechanical properties combined with healing at moderate temperatures in other polymer classes as well.

**SUPPORTING INFORMATION**

Additional characterization of all the polymers from the main text, including the reference polymer. This material is available free of charge via the Internet at http://pubs.acs.org.

**AUTHOR INFORMATION**

**Corresponding Author**

*E-mail: s.j.garciaespallargas@tudelft.nl (S. J. G.).

**Author Contributions**

All the authors contributed equally to this work.

**Notes**

The authors declare no competing financial interest.

## Acknowledgements

The authors acknowledge the financial support from the Dutch IOP program on self-healing materials under grant number IOP-SHM-012036. We acknowledge our industrial partners Tata Steel Nederland BV and Croda Nederland BV, especially the sustained support and valuable discussions with Dr Angela Smits (Croda). Many thanks to Dr Johan Bijleveld and Wouter Vogel (NovAM, TU Delft) for valuable discussions and support in the polymer synthesis and GPC analysis. We thank Ruud Hendrikx for performing the WAXS and Dr Giuseppe Portale (Groningen University) for performing the SAXS measurements.

## References

This article references 52 other publications.


(1) Döhler, D.; Michael, P.; Binder, W. H. Principles of Self-Healing Polymers. In *Self-Healing Polymers: From Principles to Applications*; Binder, W. H., Ed.; Wiley-VCH: Weinheim, 2013; pp 7-60.

(2) Zhong, N.; Post, W. Self-repair of Structural and Functional Composites with Intrinsically Self-Healing Polymer Matrices: A Review. *Compos. Part A Appl. Sci. Manuf.* **2015**, *69*, 226–239.

(3) Kuhl, N.; Bode, S.; Bose, R. K.; Vitz, J.; Seifert, A.; Hoeppener, S.; Garcia, S. J.; Spange, S.; Van der Zwaag, S.; Hager, M. D.; Schubert, U. S. Acylhydrazones as Reversible Covalent Crosslinkers for Self-Healing Polymers. *Adv. Funct. Mater*. **2015**, *25*, 3295–3301.

(4) Van der Zwaag, S. An Introduction to Material Design Principles: Damage prevention versus Damage Management. In *Self-Healing Materials: An Alternative Approach to 20 Centuries of Materials Science;* Van der Zwaag, S., Ed.; Springer: Dordrecht, 2007; pp 8-9.

(5) Garcia, S. J.; Fischer, H.R.; Van Der Zwaag, S. A Critical Appraisal of the Potential of Self Healing Polymeric Coatings. *Prog. Org. Coat.* **2011,** *72*(3), 211-221.

(6) Garcia, S.J. Effect of Polymer Architecture on the Intrinsic Self-Healing Character of Polymers. *Eur. Polym. J.* **2014**, *53*, 118-125.

(7) Cristea, M.; Ionita, D.; Hulubei, C.; Popovici, D.; Simionescu, B. C. Chain Packing Versus Chain Mobility in Semialiphatic BTDA-based Copolyimides. *Polymer* **2011**, *52*(8), 1820-1828.

(8) Eichstadt, A. E.; Ward, T. C.; Bagwell, M. D.; Farr, I. V.; Dunson, D. L.; McGrath, J. E. Synthesis and Characterization of Amorphous Partially Aliphatic Polyimide Copolymers Based on Bisphenol-A Dianhydride. *Macromolecules* **2002,** *35*(20), 7561-7568.

(9) Wakita, J.; Jin, S.; Shin, T. J.; Ree, M.; Ando, S. Analysis of Molecular Aggregation Structures of Fully Aromatic and Semialiphatic Polyimide Films with Synchrotron Grazing Incidence Wide-Angle X-ray Scattering. *Macromolecul*es **2010**, *43* (4), 1930–1941.

(10) Thiruvasagam, P. Synthesis of New Unsymmetrical Diamine and Polyimides: Structure–Property Relationship and Applications of Polyimides. *J. Polym. Res.* **2012,** *19* (9), 1-9.

(11) Thiruvasagam, P. Synthesis and Characterization of AB-type Monomers and Polyimides: A Review. *Des. Monomers Polym.* **2013,** *16* (3), 197-221.

(12) Dingemans, T. J.; Mendes, E.; Hinkley, J. J.; Weiser, E. S.; StClair, T. L. Poly(ether imide)s from Diamines with Para-, Meta-, and Ortho-Arylene Substitutions: Synthesis, Characterization, and Liquid Crystalline Properties. *Macromolecules* **2008**, *41* (7), 2474–2483.

(13) Yokota, K.; Abe, S.; Tagawa, M.; Iwata, M.; Miyazaki, E.; Ishizawa, J. I.; Kimoto, Y.; Yokota, R. Degradation Property of Commercially Available Si-containing Polyimide in Simulated Atomic Oxygen Environments for Low Earth Orbit. *High Perform. Polym.* **2010**, *22* (2), 237-251.

(14) Lei, X.F.; Chen, Y.; Zhang, H. P.; Li, X. J.; Yao, P.; Zhang, Q. Y. Space Survivable Polyimides with Excellent Optical Transparency and Self-Healing Properties Derived from Hyperbranched Polysiloxane. *ACS Appl. Mater. Interfaces* **2013**, *5* (20), 10207-10220.

(15) Périchaud, A. A.; Iskakov, R. M.; Kurbatov, A.; Akhmetov, T. Z.; Prokohdko, O. Y.; Razumovskaya, I. V.; Bazhenov, S. L.; Apel, P. Y.; Voytekunas, V. Y.; Abadie, M. J. M. Auto-Reparation of Polyimide Film Coatings for Aerospace Applications Challenges & Perspectives. In *High Performance Polymers – Polyimides Based – From Chemistry to Applications*; Abadie, M. J. M., Ed.; InTech: Rijeka, 2012; pp. 215-244.

(16) Jolley, S.T.; Williams, M. K.; Gibson, T. L.; Smith, T. M.; Caraccio, A. J.; Li, W. Self-Healing Polymer Materials for Wire Insulation, Polyimides, Flat Surfaces, and Inflatable Structures. U.S. Patent 20,120,321,828 A1, December 20, 2012.

(17) Smits, A. L. M.; Van Triet, R. B.; Dingemans, T. J.; Garcia-Espallargas, S. J.; Polyimide composition. WO Patent 2,014,029,966 A1, February 27, 2014.

(18) Susa, A.; Van der Zwaag, S.; Garcia, S. J. Room temperature self-healing polyetherimides based on a long chain aliphatic diamine. In *Self-healing materials – Pioneering research in the Netherlands;* Van der Zwaag, S.; Brinkman, E., Eds.; IOS Press: Amsterdam, 2015**;** pp 19-26.

(19) Cordier, P.; Tournilhac, F.; Soulié-Ziakovic, C.; Leibler, L. Self-Healing and Thermoreversible Rubber from Supramolecular Assembly. *Nature* **2008**, *451*, 977-980.

(20) Lutz, A.; Van der Berg, O.; Van Damme, J.; Verheyen, K.; Bauters, E.; De Graeve, I.; Du Prez, F. E.; Terryn, H. A Shape-Recovery Polymer Coating for the Corrosion Protection of Metallic Surfaces. *ACS Appl. Mater. Interfaces* **2015**, *7*, 175−183.

(21) Aboudzadeh, A.; Fernandez, M.; Muñoz, M. E.; Santamaría, A.; Mecerreyes, D. Ionic Supramolecular Networks Fully Based on Chemicals Coming from Renewable Sources. *Macromol. Rapid Commun.* **2014,** *35*, 460−465.

(22) Yamaguchi, M.; Ono, S.; Terano, M. Self-Repairing Property of Polymer Network with Dangling Chains. *Mater. Lett.* **2007,** *61*, 1396–1399.

(23) Yamaguchi, M.; Ono, S.; Okamoto, K. Interdiffusion of Dangling Chains in Weak Gel and its Application to Self-Repairing Material. *Mater. Sci. Eng. B* **2009**, *162*, 189–194.

(24) Yamaguchi, M.; Maeda, R.; Kobayashi, R.; Wada, T.; Ono, S.; Nobukawa, S. Autonomic Healing and Welding by Interdiffusion of Dangling Chains in a Weak Gel. *Polym. Int.* **2012**, *61*, 9–16.

(25) Takekoshi, T. Synthesis of Polyimides. In *Polyimides: Fundamentals and applications*; Ghosh, M. K.; Mittal, K. L., Eds.; Marcel Dekker, Inc.: New York, 1996; pp. 7-44.

(26) Soroko, I.; Bhole, Y.; Livingston, A. G. Environmentally Friendly Route for the Preparation of Solvent Resistant Polyimide Nanofiltration Membranes. *Green Chem.* **2011**, *13*, 162-168.

(27) Wang, H. H.; Wu, S.-P. Thermal and Thermo-Oxidative Degradation Properties of Poly(benzimidazole amide imide) Copolymers. *J. Appl. Polym. Sci.* **2004**, *93*(5), 2072–2081.

(28) Lee, Y.-L.; Sung, P.-H.; Liu, H.-T.; Chou, L.-C.; Ku, W.-H. Dangling Polymer Networks: Glass Transition of PU Elastomers. *J. Appl. Polym. Sci*. **1993**, *49*, 1013-1018.

(29) Lei, T.; Wang, J.-Y.; Pei, J. Design, Synthesis, and Structure–Property Relationships of Isoindigo-Based Conjugated Polymers. *Acc. Chem. Res*. **2014**, *47* (4), 1117–1126.

(30) Herbst, F.; Döhler, D.; Michael, P.; Binder, W. H. Self-Healing Polymers via Supramolecular Forces. *Macromol. Rapid Commun.* **2013**, *34*, 203-220.

(31) Müller, M.; Seidel, U.; Stadler, R. Influence of Hydrogen Bonding on the Viscoelastic Properties of Thermoreversible Networks: Analysis of the Local Complex Dynamics. *Polymer* **1995**, *36*, 3143-3150.

(32) Callies, X.; Fonteneau, C.; Véchambre, C.; Pensec, S.; Chenal, J. M.; Chazeau, L.; Bouteiller, L.; Ducouret, G.; Creton, C. Linear Rheology of Bis-Urea Functionalized Supramolecular Poly(butylacrylate)s: Part I – Weak Stickers. *Polymer* **2015**, *69*, 233-240.

(33) Callies, X.; Véchambre, C.; Fonteneau, C.; Pensec, S.; Chenal, J. M.; Chazeau, L.; Bouteiller, L.; Ducouret, G.; Creton, C. Linear Rheology of Supramolecular Polymers Center-Functionalized with Strong Stickers. *Macromolecules* **2015**, *48*, 7320-7326.

(34) Trinkle, S.; Friedrich, C. Van Gurp-Palmen-Plot: a Way to Characterize Polydispersity of Linear Polymers. *Rheol. Acta* **2001**, *40*, 322-328.

(35) Trinkle, S.; Walter, P.; Friedrich, C. Van Gurp-Palmen Plot II – Classification of Long Chain Branched Polymers by Their Topology. *Rheol. Acta* **2002**, *41*, 103.

(36) Kramer, O.; Greco, R.; Neira, R. A.; Ferry, J. D. Rubber Networks Containing Unattached Macromolecules. I. Linear Viscoelastic Properties of the System Butyl Rubber–Polyisobutylene. *J. Polym. Sci. Part B Polym. Phys.* **1974**, *12*, 2361-2374.

(37) Yount, W. C.; Loveless, D. M.; Craig, S. L Strong Means Slow: Dynamic Contributions to the Bulk Mechanical Properties of Supramolecular Networks*. Angew. Chem. Int. Ed. Eng.* **2005**, *44*, 2746-2748.

(38) Stadler, F. J.; Pyckhout-Hintzen, W.; Schumers, J.-M.; Fustin, C.-A.; Gohy, J.-F.; Bailly, C. Linear Viscoelastic Rheology of Moderately Entangled Telechelic Polybutadiene Temporary Networks. *Macromolecules* **2009**, *42*, 6181-6192.

(39) Bose, R. K.; Hohlbein, N.; Garcia, S. J.; Schmidt, A. M.; Van der Zwaag, S. Connecting Supramolecular Bond Lifetime and Network Mobility for Scratch Healing in Poly(butyl acrylate) Ionomers Containing Sodium, Zinc and Cobalt. *Phys. Chem. Chem. Phys.* **2015**, *17*, 1697-1704.

(40) Herbst, F.; Seiffert, S.; Binder, W. H. Dynamic Supramolecular Poly(isobutylene)s for Self-Healing Materials. *Polym. Chem.* **2012**, *3*, 3084-3092.

(41) Aboudzadeh, M. A.; Muñoz, M. E.; Santamaría, A.; Fernández-Berridi, M. J.; Irusta, L.; Mecerreyes, D. Synthesis and Rheological Behavior of Supramolecular Ionic Networks Based on Citric Acid and Aliphatic Diamines. *Macromolecules* **2012**, *45*, 7599-7606.

(42) Graessley, W. W. *Polymeric Liquids & Networks: Dynamics and Rheology*; Taylor & Francis Inc.: London, 2004.

(43) Knoben, W.; Besseling, N. A. M.; Bouteiller, L.; Cohen Stuart, M. A. Dynamics of Reversible Supramolecular Polymers: Independent Determination of the Dependence of Linear Viscoelasticity on Concentration and Chain Length by Using Chain Stoppers. *Phys. Chem. Chem. Phys.* **2005**, *7*, 2390-2398.

(44) Ahmadi, M.; Hawke, L. G. D.; Goldansaz, H.; van Ruymbeke, E. Dynamics of Entangled Linear Supramolecular Chains with Sticky Side Groups: Influence of Hindered Fluctuations. *Macromolecules* **2015**, *48,* 7300-7310.

(45) Green, M. S.; Tobolsky, A. V. A New Approach to the Theory of Relaxing Polymeric Media. *J. Chem. Phys.* **1946**, *14*, 80-92.

(46) Tanaka, F.; Edwards, S. F. Viscoelastic Properties of Physically Crosslinked Networks. 1. Transient Network Theory. *Macromolecules* **1992**, *25*, 1516-1523.

(47) Rubinstein, M.; Semenov, A. N. Thermoreversible Gelation in Solutions of Associating Polymers. 2. Linear Dynamics. *Macromolecules* **1998**, *31*, 1386-1397.

(48) Grande, A. M.; Garcia, S.J.; Van der Zwaag, S. On the Interfacial Healing of a Supramolecular Elastomer. *Polymer* **2015**, *56*, 435-442.

(49) Grande, A. M.; Bijleveld, J. C.; Garcia, S. J.; Van der Zwaag, S. A Combined Rheological Fracture Mechanical–Rheological Study to Separate the Contributions of Hydrogen Bonds and Disulphide Linkages to the Healing of Poly(urea-urethane) Networks. *Polymer* **2016**, *96*, 26-34.

(50) Chen, Y.; Kushner, A. M.; Williams, G. A.; Guan, Z. Multiphase Design of Autonomic Self-Healing Thermoplastic Elastomers. *Nat. Chem.* **2012**, *4*, 467–472.

(51) Rekondo, A.; Martin, R.; Ruiz de Luzuriaga, A.; Cabañero, G.; Grande, H. J.; Odriozola, I. Catalyst-free Room-Temperature Self-healing Elastomers Based on Aromatic Disulfide Metathesis. *Mater. Horiz.* **2014**, *1*, 237-240.

(52) Bode, S.; Enke, M.; Hernandez, M.; Bose, R. K.; Grande, A. M.; van der Zwaag, S.; Schubert, U. S.; Garcia, S. J.; Hager, M. D. Characterization of self-healing polymers: From macroscopic healing tests to the molecular mechanism. *Adv. Polym. Sci.*, **2016**, *273*, 113-142.

Graphical Abstract; For Table of Contents Only :